C. R. Mecanique 346 (2018) 1233–1252

Contents lists available at ScienceDirect

Comptes Rendus Mecanique

www.sciencedirect.com

Effect of particle shape on micro- and mesostructure evolution of granular assemblies under biaxial loading conditions

Jianqiu Tian [a], Enlong Liu [a,b,*]

[a] State Key Laboratory of Hydraulics and Mountain River Engineering, College of Water Resource & Hydropower, Sichuan University, Chengdu 610065, China

[b] Northwest Institute of Eco-Environment and Resources, State Key Laboratory of Frozen Soil Engineering, Chinese Academy of Sciences, Lanzhou, Gansu 730000, China

ARTICLE INFO

Article history:
Received 26 April 2018
Accepted 29 August 2018
Available online 18 September 2018

Keywords:
Particle shape
Biaxial simulation
Particle rotation
Fabric evolution
Loops evolution
Modified clustering coefficient
Complex network

ABSTRACT

Discrete element method (DEM) numerical biaxial tests on samples with different particle shapes are performed to investigate how the multiscale evolves with varying particle shape. The samples used in such simulations are composed of circular, square, and elongated particles, respectively. For the numerical results, analyses are conducted in terms of microscopic evolution, i.e. particle rotation and evolution of fabric, and mesoscopic evolution, i.e. the evolution of loops and improved clustering coefficient. At the microscale, the mean particle rotation of circular particles is remarkably larger than those of square and elongated particles, and the shear band localization phenomenon is more obvious when the aspect ratio (AR) decreases. Considering the fabric evolving with particle shape, the value of anisotropy gradually increases when particle shape becomes irregular, and contacts of circular particles are pronouncedly less than those of irregular particles from the coordination number and curves of degree distribution. At the mesoscale, when the particle relationship is considered, the isotropic particles (i.e. circular and square particles) have similar evolutions of loops and modified clustering coefficient, whereas the elongated particles have remarkable three loops and modified clustering coefficient, which are both larger than those of isotropic particles.

1. Introduction

Granular assemblies exist in nature extensively. Human activities are intimately linked to the properties of granular assemblies, such as debris-flow, mining, and damming engineering. Such materials have various particle shapes. Particle shape has dramatic effect on the macro-, meso-, and micro-properties of granular materials. For example, Hidalgo et al. [1] find that stress propagation is strongly affected by the grains elongation, and Nouguier-Lehon [2] exhibits that the cumulative rotations of discs are higher than those of polygons and that the stress–strain relations are diverse with different particle shapes. At the macroscale, strength and deformation are usually discussed. At the mesoscale, the particle relations of a particle cluster are usually considered. At the microscale, the contact information and property for single particles are

* Corresponding author at: Northwest Institute of Eco-Environment and Resources, State Key Laboratory of Frozen Soil Engineering, Chinese Academy of Sciences, Lanzhou, Gansu 730000, China.
E-mail address: liuenlong@scu.edu.cn (E. Liu).

https://doi.org/10.1016/j.crme.2018.08.013
1631-0721/

usually analyzed. Hence, the physical mechanisms for the particle shape affecting granular materials on the multiscale have always caught the interest of many researchers [3–5]. How the particle shape affects the behavior of granular materials is not clear till now, such as the rolling of particles varying with the particle shape, the fabric of granular materials affected by the particle shape. Thus, the influence of particle shape on the properties of granular materials remains an open topic till now. Different methods are carried out to explore the physical mechanisms. On the one hand, there are some researchers using traditional laboratory tests (such as direct shear tests, simple shear tests, and triaxial tests) to explore the role of particle shape in granular materials, such as Shinohara et al. [6], Sukumaran and Ashmawy [7], Cho et al. [8], Yang and Wei [9], and Yang and Luo [10], while such traditional laboratory tests only can be used to research the macro-properties of granular materials. If the microscopic information is collected in traditional laboratory experiments, other assistive technologies, such as CT scan, X-ray, and electron microscopy, are needed. On the other hand, with the development of discrete element method (DEM) [11], the micro- and mesostructure in granular materials can easily be analyzed, and complex load-paths are controlled more easily by DEM than in traditional tests. Furthermore, the irregular particles can be studied in DEM with computational efficiency promotion. Therefore, some researchers use DEM to explore the effect of particle shape on the micro- and mesostructure evolution of granular materials. For example, Nguyen et al. [12] used the contact dynamics method to analyze the combined effect of polydispersity, both in particle size and in particle shape, on the shear strength and microstructure of sheared granular materials composed of pentagonal particles. De Bono and McDowell [13] performed one-dimensional normal compression of non-spherical particles with PFC. With this simulation, the non-spherical particles are shown to give the clumps a lower coefficient of lateral earth pressure at rest, and a lower Poisson ratio compared to the spheres. And there are also other researchers using DEM to analyze the effect of particle shape on granular materials [14–17]. In these simulations, few references discuss the macro-properties through micro- and mesoscales, which may provide a new approach for formulating the stress–strain relationship in granular materials. Thus, some new viewpoints at the micro- and mesoscale are needed to research the effect of particle shape on granular materials.

At the microscale, fabric evolution is usually discussed both with circular (or spherical) and non-circular (or non-spherical) particles [18,19]. Particle rotation in the sample is usually analyzed with circular and spherical particles [20]. It is less discussed for fabrics with non-circular and non-spherical particles. Whereas particle rotation is the main style of particle movement, the effect of particle shape on particle rotation can be used to justify the rolling resistance parameters introduced to counterbalance the spherical simplification of the grains geometry in DEM simulations [21–23], and other particle shapes excepting regular polygonal particles that have been researched can be used to compare with circular particles [21]. Thus, particle rotation varying with particle shape is worth discussing. When the macro-properties are discussed, not only the single particle and contacts are worth noting, but also the rearrangement of the particles is the key point. Hence, at the meso-scale, the topologic structure is worth noting. Furthermore, loops dominate the network of the specimen. Some works have been done in this aspect. For instance, Tordesillas et al. [24] examined the coevolution of N loops and force chains with circular particles. Zhu et al. [25,26] investigated how the mesoscopic loops evolve along the drained biaxial loading path by DEM with circular particles, whereas few non-circular and non-spherical particles are used to explore the evolution of loops. Recently, complex networks, which are a very useful mathematical tool to investigate how the structure and the organization of granular systems change [27], are used to describe some characters of granular materials. Whereas, for granular materials, particles too far from each other have no chance to be in contact directly, this may not be the case for other types of networks. Complex networks need to be modified when granular materials are researched. Walker and Tordesillas [28], and Tordesillas et al. [29] explored the samples composed of circular particle using a complex network perspective. Tian et al. [17] applied complex networks in the research of particle shape under direct shear conditions, while other methods in complex networks are still worth exploring combined with particle shape, and they need be improved to reflect the characters of granular networks.

The discussion about the role of particle shape in particle rotation is lacking. And few researches adopt loops and complex networks to explore the mechanisms for particle shape affecting the mechanical properties of granular materials. In a word, the effect of particle shape on the multiscale evolution of granular assemblies is worth noting till now. Hence, in this paper, we propose the circular, square, and elongated particles to be explored in biaxial simulations with DEM, respectively. This is stated in Sect. 2. In Sect. 3, according to biaxial simulations, the macro properties, i.e. strength and deformation, and the micro properties, i.e. particle rotation and fabric evolution, of granular materials are discussed. Then in Sect. 4, the evolution of mesoscale for different particle shapes is explored. To explore the evolution of irregular particles, the loops are improved. The definition of the clustering coefficient in complex networks is modified to reflect the character of granular materials. In Sect. 5, the effect of particle shape on the multiscale evolution of granular materials is summarized.

2. Numerical simulation

2.1. Particle shape definition

In this paper, the properties of granular materials are simulated by using the program PFC^{2D}. Circular, square, and elongated particles are adopted in the simulations and their shapes gradually become irregular (see Fig. 1a). There is no main axis in circular or square particles, so they are defined as isotropic particles. Similarly, there is a main axis in the elongated particle, so it is defined as the anisotropic particle. In order to define these differences of particle shapes, the aspect ratio (AR) proposed by Altuhafi et al. [30] is adopted in the simulations. Referring to Fig. 1b, AR can be calculated as the

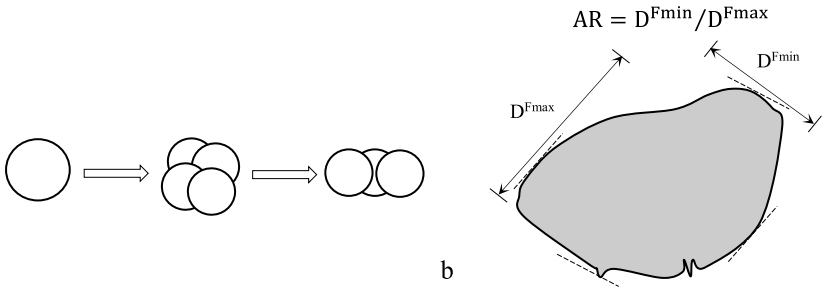

Fig. 1. Particle shape definition: (a) the three types of particle used in simulations; (b) definition of the aspect ratio (AR).

Table 1
Model parameters in DEM simulations.

Parameter	Value
Particle size (radius)	0.3–0.6 mm
Particle density	2630 kg/m^3
Damping coefficient	0.7
Particle friction (biaxial tests only)	0.5
Wall friction	0
Particle/wall and particle/particle normal stiffness	1.5×10^8 N/m
Particle/wall and particle/particle shear stiffness	1.0×10^8 N/m

Table 2
Porosity results for different types of specimens.

	Specimen of circular particles	Specimen of square particles	Specimen of elongated particles
n_{max}	0.210	0.193	0.171
n_{min}	0.164	0.136	0.115
n	0.178	0.154	0.133

minimum divided by the maximum Feret diameters, and the Feret diameter can be measured as the distance between two tangents on opposite sides of the particle. From the definition of AR, it is clear that AR is sensitive to the elongation of the particle. The definition of the aspect ratio is used to calculate the circular, square, and elongated particles in simulations. Their values of AR are calculated as 1.00, 0.88, and 0.50, respectively.

2.2. Test preparation

The granular assemblies with different particle shapes have different ranges of void ratios. When the influence of particle shape on granular materials are considered, the void ratio used to control the granular materials is not reasonable. Hence, the relative density (D_r) is used to control three types of assemblies that are constituted by circular, square, and elongated particles, respectively. And the relation between porosity (n) and relative density is illustrated as follows:

$$D_r = (1 - n_{min})(n_{max} - n)/\left[(1 - n)(n_{max} - n_{min})\right] \tag{1}$$

where n_{min} is the minimum porosity of the granular assembly and n_{max} is the maximum porosity of the granular assembly. The n_{max} and n_{min} values of different granular assemblies are obtained by simulating the relative density test of coarse-grained soils, which can refer to the specification of soil test [31]. The model parameters used in the relative density test, referring to Tian et al. [17], are illustrated in Table 1 (note: there is no friction in the relative density test to improve the computation cost, and it has little effect on the result of n_{max} and n_{min}). The linear model in PFC^{2D} is used in this test and the range of particle size is drawn from uniform distributions throughout the model domain. These parameters are also used in biaxial tests that will be introduced later. At last, the simulated results of n_{max} and n_{min} are shown in Table 2. And the 70% relative density translated to porosities of different particle shapes are shown in the last row of Table 2. Table 2 shows both n_{max} and n_{min} to decrease when AR decreases.

2.3. Biaxial simulation

The process of performing the biaxial simulation is illustrated here. At first, four walls are generated, with dimensions 80 mm (height) × 40 mm (width). According to the porosities displayed in Table 2, the radii of clumps ranging from 0.3 to

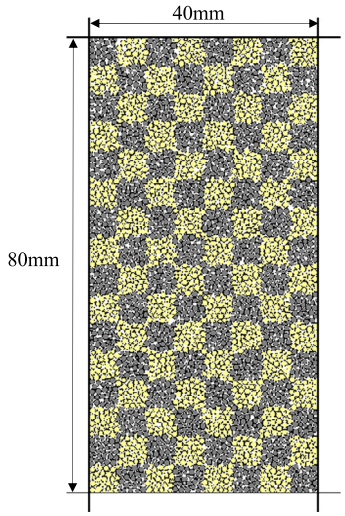

Fig. 2. DEM specimen after generation.

0.6 mm are generated in the walls. There are 3947 particles in the sample with circular particles, there are 4070 particles in the sample with square particles, and there are total 4182 particles in the sample with elongated particles (the number of particles is mainly limited by the computational efficiency of DEM and data processing of the loop in the latter, and it is large enough that we can study the properties of granular materials). Circular, square, and elongated particles have the same range of size, and sample generation is controlled by relative density, so there are a comparable number of particles in different samples. The initial state of a specimen is illustrated in Fig. 2. Then, the confining pressure (200 kPa, 400 kPa, and 600 kPa) is applied on the specimen through four walls. When the target of the confining pressure is attained, the top and bottom walls are moved with constant down and up velocities, respectively. The value of this velocity is 0.8 mm/s. To ensure the quasi-static condition, the inertia parameter I [32,33] is adopted as follows:

$$I = \dot{\varepsilon}\sqrt{m/p} \tag{2}$$

where $\dot{\varepsilon}$ is the shear strain rate, m is the mean particle mass, and p is the confining pressure. The quasi-static condition is characterized by $I \ll 1$. In the biaxial simulations, the inertia parameter I is below 2.0×10^{-6}, which is low enough to ensure the quasi-static condition. At last, shear ceases when the axial strain attains 20%.

3. Macromechanical properties and microanalyses

3.1. Mechanical properties in the macroscale

Fig. 3 shows the relations between the deviatoric stress ($\sigma_1 - \sigma_2$) and the axial strain (ε_1), and the volumetric strain (ε_v) of the samples varying with the axial strain (ε_1) is also illustrated in Fig. 3. As we can see, the deviatoric stresses of circular, square and elongated particles all exhibit a peak followed by a softening reaching the critical state. And all the volumetric strains are compressed firstly, then followed by dilatancy; at last, the critical state is achieved. Because of that, the samples used in the simulations are all dense.

Under the same confining pressure, the influence of particle shape on the macro-mechanical properties is analyzed here. Fig. 3 shows that the peak and the residual deviatoric stresses both increase when the particle shape is irregular. This phenomenon can be explained as follows. As the sample is sheared, the particles in the sample have two styles to move, which are sliding and rolling. Contacts of different particle shapes are illustrated in Fig. 4, where there is only one contact between two circular particles, and there are two or more contacts between two irregular particles. The increasing number of contacts around one particle can enhance the sliding constraint and rolling resistance of it. To move irregular particles, greater force will be applied. And the elongation of the particle can obstruct the rolling of the particle, so the particle rolls harder when AR decreases. The circular particles have less contacts than irregular particles, and the circular particle has the largest aspect ratio ($AR = 1.00$) among the three shapes used in simulations. Therefore, the sample with circular particles has the lowest peak and residual deviatoric stresses among all the curves. The square particles and elongated particles have more contacts than the circular particles, whereas the square particle has the intermediate aspect ratio ($AR = 0.88$). And the elongated particle has the smallest aspect ratio ($AR = 0.50$) among these three particle shapes. Hence, the sample with square particles has intermediate peak and residual deviatoric stresses, and the sample with elongated particles has the largest peak and residual deviatoric stresses. On the other hand, the value of dilatancy at steady state increases when particle shape becomes irregular. The volumetric strain of the sample is related to the space constructed by the particles

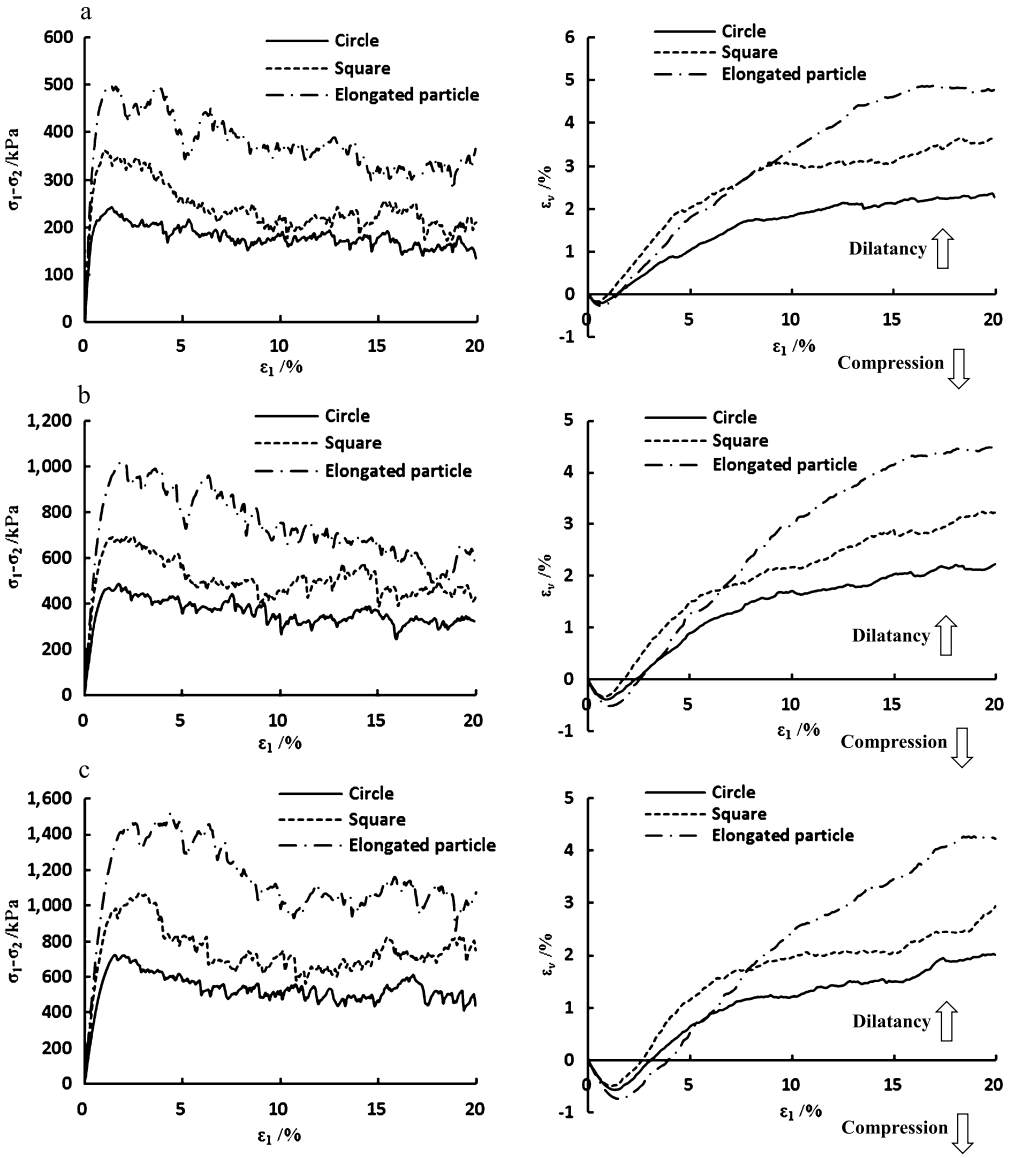

Fig. 3. Relation between the deviatoric stress and the axial strain, and the volumetric strain of samples varying with the axial strain: (a) confining pressure, 200 kPa; (b) confining pressure, 400 kPa; (c) confining pressure, 600 kPa.

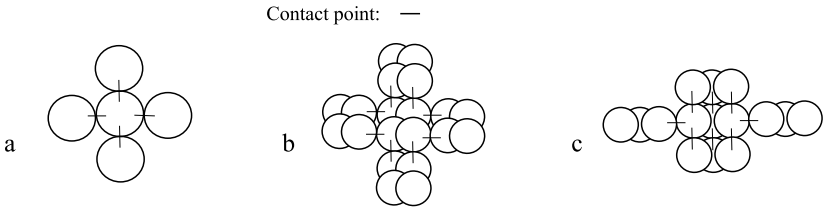

Fig. 4. Contacts between particles: (a) circular particles; (b) square particles; (c) elongated particles.

in it. Considering the AR of three particle shapes used in the simulations, when AR decreases, particle rolling needs more space. Hence, the dilatancy of the elongated particle is the largest, and the dilatancy of the circular particles is the smallest among the three particle shapes.

For the same particle shape, the effect of different confining pressures is considered here. The curve of deviatoric stress varying with axial strain moves up when the confining pressure increases, and the amount of compression increases and the dilatancy decreases when the confining pressure increases. Such a phenomenon can be explained as follows. With the

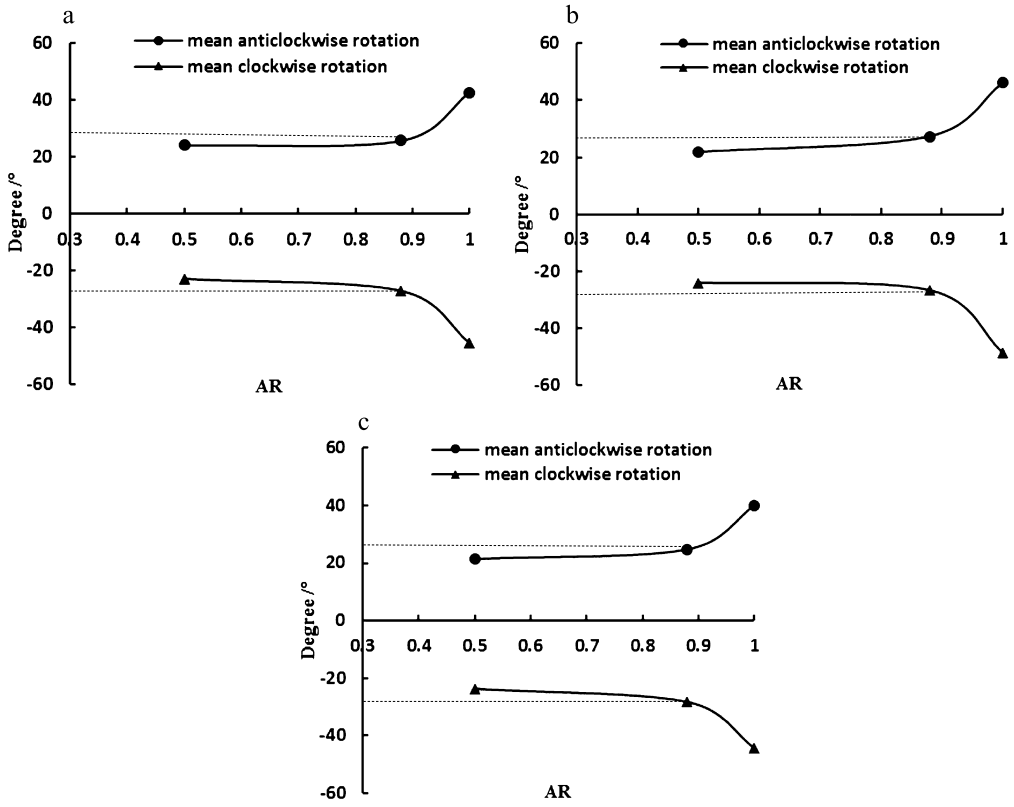

Fig. 5. Mean rotation of particles with different particle shapes at the critical state: (a) confining pressure, 200 kPa; (b) confining pressure, 400 kPa; (c) confining pressure, 600 kPa.

confining pressure growing up, contacts among particles are stronger than those at low confining pressure. Hence, under high confining pressure, greater force is needed to make particles move (i.e. the peak and residual deviatoric stresses both increase when the confining pressure increases). On the other hand, the high confining pressure helps to compress the space among particles, thus the amount of compression increases when the confining pressure increases. And under high confining pressure, the space is constructed harder when axial strain increases, so the dilatancy of the samples decreases when the confining pressure increases. This result is the same in other researches, such as those of Alonso-Marroquin et al. [34], Bi et al. [35], and Hama et al. [36].

3.2. Particle rotation at the critical state

It is well known that rotation is an important pattern of particle movements and that there is much interest to find its effect on granular materials [37–39]. Thus, at the critical state with a larger axial strain, the differences of particle rotation among circular, square, and elongated particles are explored here. The mean clockwise rotation and the mean counterclockwise rotation of the three types of particle shapes are calculated, respectively. These values are illustrated in Fig. 5. As we can see, not only the absolute values for the mean clockwise rotation increase when AR increases (the particle shape gradually becoming regular), but the mean counterclockwise rotation follows the same trend by varying AR. On the one hand, the circular particle is isotropic and has less contact points to constrain it than the irregular particles have. There are less constraints for the circular particle among the three types of particle shapes, so it has the maximum values of the mean rotation. On the other hand, the elongated particle is anisotropic and has a mass of contacts around it. Hence, it has the minimum values of the mean rotation.

The particles with rotation exceeding the mean rotation values are shown in Fig. 6. For the circular, square, and elongated particles, their rotations exceeding their mean clockwise rotations, respectively, are indicated by black particles, and their rotations exceeding their mean counterclockwise rotations, respectively, are indicated by orange particles. The clockwise rotation is dominant in the direction that dips to the left side. The counterclockwise rotation is dominant in the direction that dips to the right side. This pattern of particle rotation is similar to the strain localizations of Iwashita and Oda [37] and O'Sullivan et al. [38], which is more obvious when the confining pressure increases.

The observed difference about particle rotation in Fig. 6 can be explained as follows: at the critical state, the plot of displacement vectors is shown in Fig. 7. As we can see that the displacement gradually decreases with particles getting closer to the center of the sample. When the displacements around one particle are not consistent, the particle will rotate,

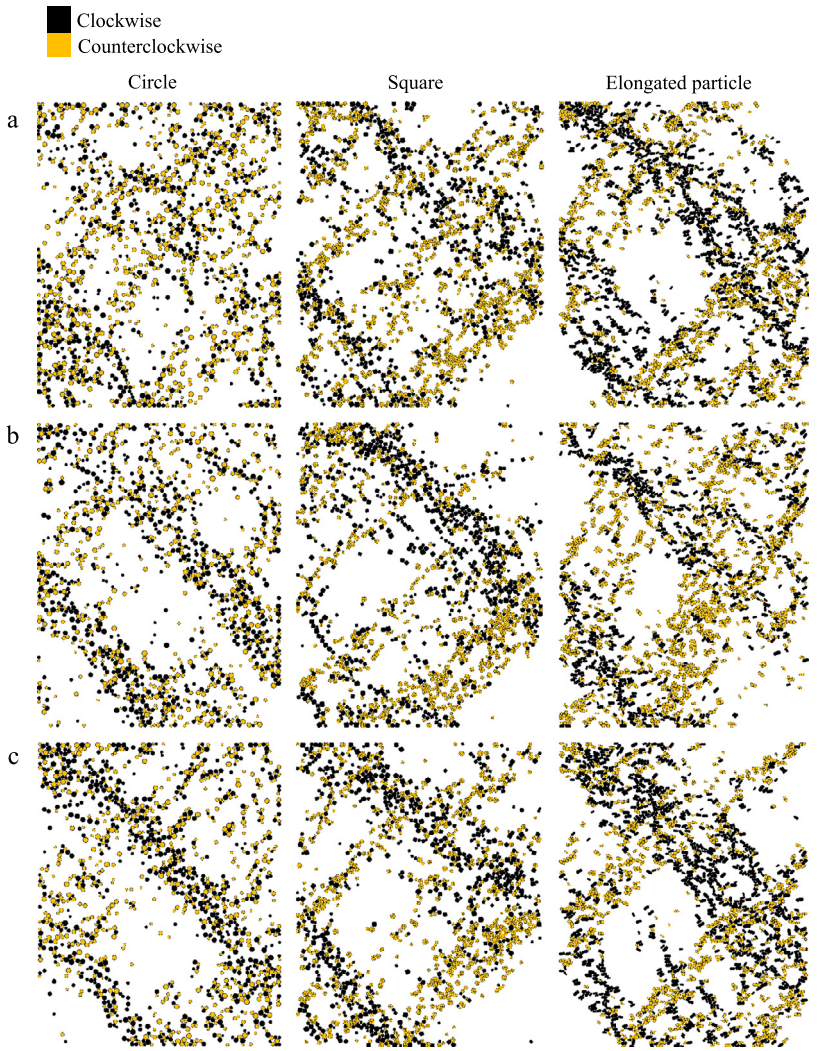

Fig. 6. Distribution of rotation whose magnitude exceeds the mean clockwise or counterclockwise rotation at the critical state: (a) confining pressure, 200 kPa; (b) confining pressure, 400 kPa; (c) confining pressure, 600 kPa.

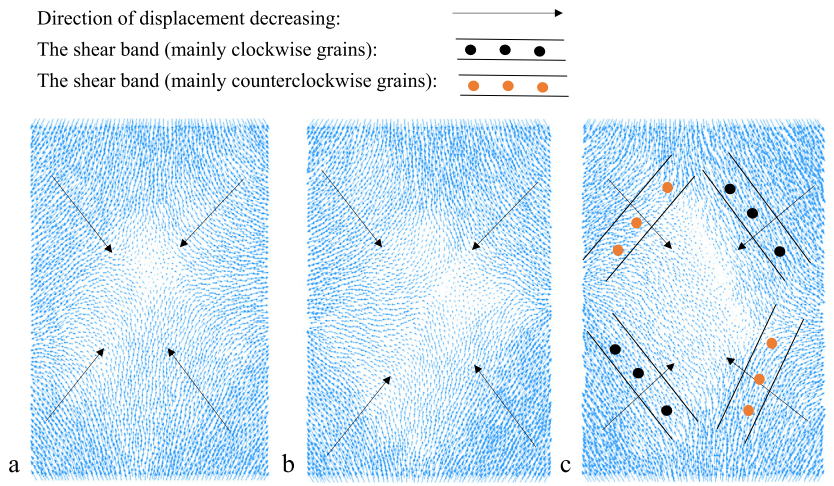

Fig. 7. At the critical state, plot of displacement vectors under a confining pressure of 200 kPa: (a) sample with circular particles; (b) sample with square particles; (c) sample with elongated particles.

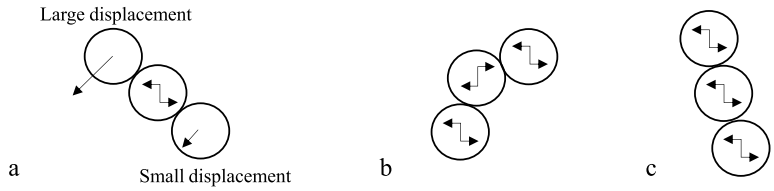

Fig. 8. Reason for and mechanisms of particle rotation: (a) reason of particle rotation; (b) weak constraint: clockwise rotation accompanied with counterclockwise rotation; (c) strong constraint: formed column-like structure.

as shown in Fig. 8a. And the gradients of displacements are drawn in Fig. 7. Clockwise rotation results from the decrease of the displacement vector, which dips to the right, whereas counterclockwise rotation results from the decrease of the displacement vector, which dips to the left (the trend of displacement vectors under a confining pressure of 200 kPa is almost the same as at 400 kPa and 600 kPa, so only the 200 kPa displacement vector trend is given). Thus, clockwise rotation is dominant in the direction that dips to the left-hand side. Counterclockwise rotation is dominant in the direction that dips to the right-hand side. The displacement gradient and particle rotation are perpendicular with each other. The direction of particle rotation near the boundaries of the sample is more random than in other regions since they are influenced, not only by the gradient of displacement, but also by the boundary. Furthermore, it is well known that particle rotation plays a dominant role in the development of shear bands in granular materials [37,40]. Thus, the shear band localization phenomenon is discussed with particle rotation here. According to Fig. 6, the confining pressure of 200 kPa is discussed firstly. The circular particles that rotate by more than their mean particle rotations are dispersed so widely that the shear bands are not clear defined. For the elongated particles, such highly rotated particles are concentrated inside the shear bands. The square particles are intermediary between such two cases. So, the shear band with localization phenomenon is more obvious when AR decreases. Then increasing the confining pressure can also make particle rotate concentrated inside the shear bands. This can be explained as follows. Both the decrease of AR and the increase of the confining pressure can enhance the rolling resistance between particles. When the particles have low rolling resistance, they can roll freely. One particle rolling clockwise or counterclockwise makes its neighbors rolling in the opposite direction (Fig. 8b), because of force and reaction force. When the particles have high rolling resistance, the column-like structure (Fig. 8c) and shear bands are formed.

3.3. Anisotropy

To analyze the effect of particle shape on the contact properties of granular materials, the anisotropy of contact normal is adopted. The process of quantifying anisotropy is explained here. Firstly, the orientations of the contacts in the sample are plotted as rose diagram, whose interval of the angle is 10 degrees, and the polar axis represents the number of contact normals. Then, the second Fourier component proposed by Rothenburg and Bathurst [41] to quantify the value of anisotropy is used in the simulations. Such method is shown as follows:

$$E(\theta) = \left[1 + a\cos 2(\theta - \theta_a)\right]/2\pi \tag{3}$$

where a defines the magnitude of anisotropy, θ is the contact normal orientation between particles, and θ_a is a parameter describing the direction of anisotropy. When the parameter $a = 0$, the contact normal distribution is isotropic. The parameter a has a larger value when anisotropy increases; nevertheless, its value cannot exceed 1. The rose diagram and fitted functions $E(\theta)$ are illustrated in Fig. 9a. Rose diagrams of contact normal under confining pressures of 200 kPa, 400 kPa, and 600 kPa are illustrated in Figs. 9, 10, and 11, respectively.

The evolution of the anisotropy coefficient a with increasing the axial strain is illustrated in Fig. 12. At the initial state (axial strain 0%), the samples with three different particle shapes are all isotropic. The values of anisotropy for three particle shapes suddenly increase, when axial shearing just starts. Then the anisotropy of circular and square particles will be steady when the axial strain increases. The anisotropy of the elongated particles will slow down the rate of growth. At the critical state (axial strain 20%), the anisotropy of elongated particles is remarkably greater than that of circular and square particles, and the square particles have a larger anisotropy than circular ones. This phenomenon can be explained as follows. The samples in biaxial simulations are all generated by randomly distributed particles, and the confining pressures of the four walls loading on the sample are the same. Hence, at the initial state, the contact orientations are distributed homogeneously in the sample (i.e. at the initial state, the samples are all isotropic, as shown in Figs. 9a, 9c, 9e, 10a, 10c, 10e, 11a, 11c, and 11e). From the comparison between the initial state and the critical state, we can see that the numbers of contacts for circular, square, and elongated particles in the horizontal direction all decrease at the critical state, compared with the initial state. Along the vertical direction of the sample, the number of contacts for circular particles has few reduction, and there is a remarkable decrease in the number of square particles. But to better resist axial loading, the elongated particles (i.e. the main axis of the particle) rotate to be perpendicular to the major principal stress direction. Numerous elongated particles rotate to the state as can be seen in Fig. 4c, leading to a remarkable increase of the contacts between elongated particles in the vertical direction, and a decrease in the horizontal direction. At the critical state, the contacts of

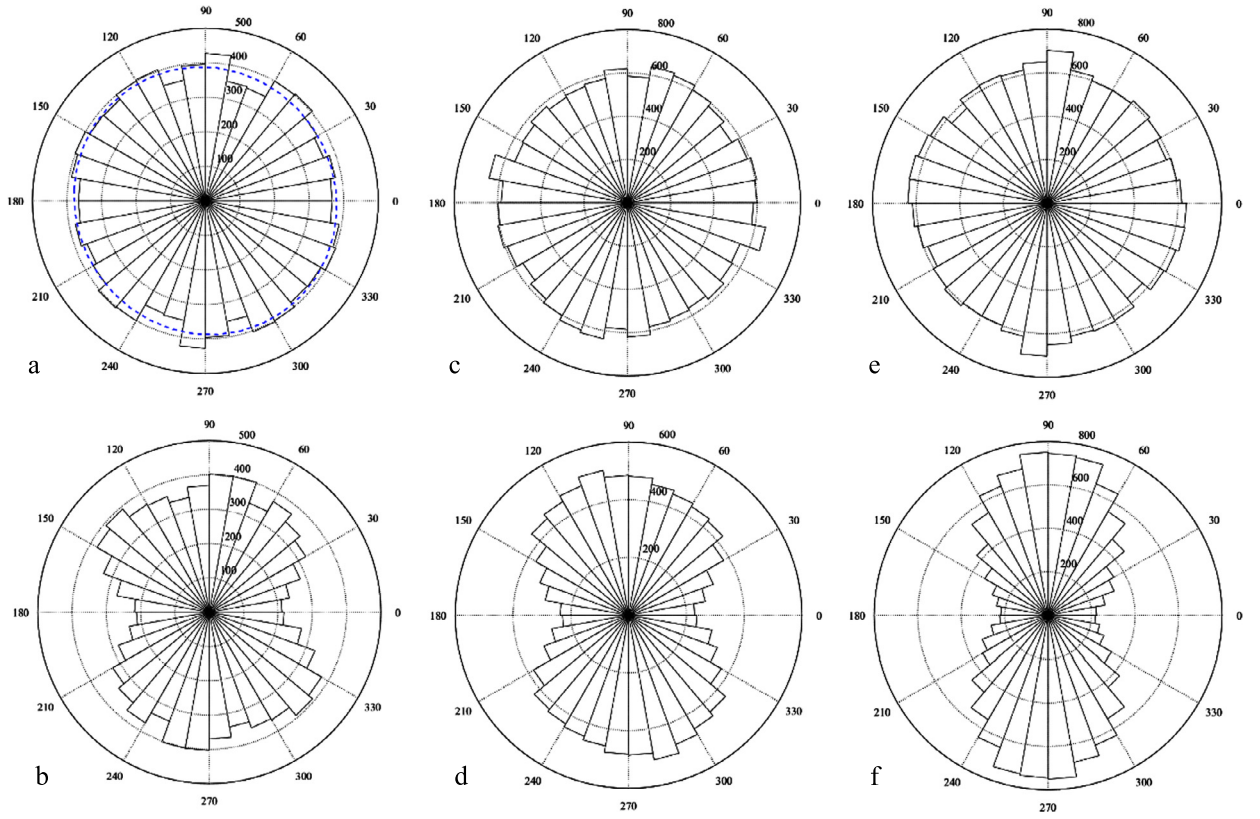

Fig. 9. Rose diagrams of contact normal with confining pressure 200 kPa: (a) circular grains at 0% of axial strain; (b) circular grains at 20% of axial strain; (c) square grains at 0% of axial strain; (d) square grains at 20% of axial strain; (e) elongated grains at 0% of axial strain; (f) elongated grains at 20% of axial strain.

circular, square, and elongated particles are almost the same in the horizontal direction. The contacts of circular particles in the vertical direction are the less numerous among the three types of particles. Along this direction, the sample with square particles has an intermediate number of contacts, and the sample with elongated particles has the largest number of contacts, as illustrated in Figs. 9b, 9d, 9f, 10b, 10d, 10f, 11b, 11d, and 11f. Thus, the anisotropy of elongated particles is greater than that of the other shapes, and that of square particles is greater than that of circular particles at the critical state. On the other hand, the directions of anisotropy for circular, square, and elongated particles are almost consistent with the direction of σ_1, at the critical state.

3.4. Degree

Here, the definition of degree, which is taken from the network theory [27], is totally the same as that of the coordination number [42]. Fig. 13a shows examples of different granular assemblies. The number of contacts around one particle is defined as the degree of this particle. For example, node 1 has three contacts, so its degree is 3. Node 2 and node 3 have 4 degrees, respectively. Then, the average degree is defined, which is the number of contacts per particle in the granular assembly, denoted by Z. The calculation of Z is as follows:

$$Z = 2N_c/N_p \tag{4}$$

where N_c is the total number of contacts, and N_p represents the number of particles. And a multiplying factor of 2 is applied, because each contact is shared by two particles.

In Fig. 14, the distributions $N_n/\sum N_n$ are illustrated. N_n represents the number of nodes with n degrees. The same sample is explored here. At the initial state, the curve of the degree distribution is located on the right side of the curves in the subsequent states. During the loading process, the curves move to the left suddenly at first, and then the curves in axial strain 10% and critical state almost coincide with each other. For the samples with circular particles, when the state transfers from initial to axial strain 10% or 20%, the percentage of 4 or higher degrees (the high degree) decreases and of 3 or lower degrees (the low degree) increases. For the samples with square particles, when the state switches from the initial to a later state, there is a decrease of 5 or higher degrees (the high degree), but there is an increase of 4 or lower degrees (the low degree). And for the sample with elongated particles, 5 or higher degrees (the high degree) decreases and 4 or

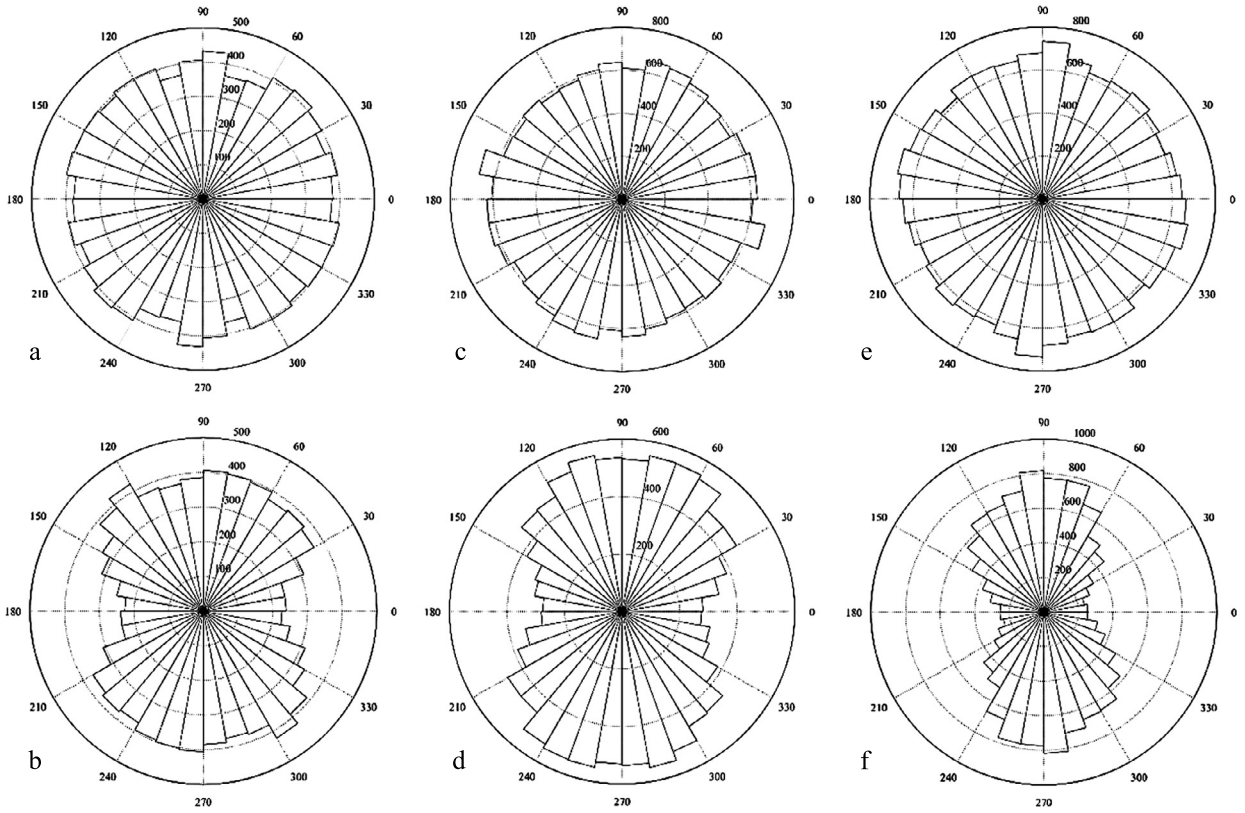

Fig. 10. Rose diagrams of contact normal with a confining pressure of 400 kPa: (a) circular grains at 0% of axial strain; (b) circular grains at 20% of axial strain; (c) square grains at 0% of axial strain; (d) square grains at 20% of axial strain; (e) elongated grains at 0% of axial strain; (f) elongated grains at 20% of axial strain.

lower degrees (the low degree) increases when the system switches from the initial to a subsequent state. Figs. 15 and 16 show the degree distribution under confining pressures 400 kPa and 600 kPa, respectively. It can be seen that the trend is almost the same as that in Fig. 14, but the confining pressure has an effect on the starting point of the high degree. Under 400 kPa and 600 kPa, the high degree of elongated particles starts from 6 degrees. Under 600 kPa, the high degree of square particles starts from 6 degrees. These results are explained here. Particle contacts in the sample decrease when the dilatancy increases. Thus, the high degree loses contacts, which are transferred to the low degree. Then the high degree decreases as the low degree increases. When the confining pressure increases, the sample is denser, resulting in more contacts around particles. So the boundary between the low degree and the high degree is increased. Fig. 17 shows the curves of the degree distribution for different particle shapes. The degree distribution of circular particles stays on the left side of the curves of other particle shapes all the time. The curves of square and elongated particles are almost the same at the initial state, but the curve of square particles is located on the left side of the one that regards the elongated particles at the critical state. The irregular particles have similar contact numbers, which are intrinsically larger than for circular ones, as illustrated in Fig. 4. Thus, the distributions of the circular particles are always on the left side of those of irregular particles. The distributions of irregular particles are consistent with each other at the initial state. At the critical state, the elongated particles have more contacts than square ones (as illustrated by Fig. 9d, 9f, 10d, 10f, 11d, and 11f), and the samples of these two shapes have similar particle numbers. So, the curve of square particles is located on the left side of the one that regards elongated particles.

The evolution of Z with the axial strain is illustrated in Fig. 18. This figure evidences that the trends of all the curves are the same. They all show an increase at first, and then decrease dramatically, whereas curves slow down with the decreasing velocity and gradually evolve steadily at last. The contacts generated in the vertical direction are more than the disappeared contacts in the horizontal direction at the initial state, the total number of contacts increasing, thus there is a peak in the curves. When the axial strain increases, the contacts generated are gradually fewer than those that had disappeared with sample compression and dilatancy, and the total number of contacts decrease, as Z. On the other hand, the Z value of circular particles is the lowest among the three particle shapes, and that of the elongated particles is the highest. Let us focus again on the contacts of the different particle shapes illustrated in Fig. 4. The contacts of circular particles are remarkably fewer than these of the other shapes. Thus, irregular particles have bigger values of Z than circular particles. Comparing the square particles with the elongated ones, we can find that the number of contacts between the particles exhibits few differences. Hence, the Z values of irregular particles are very close to each other at the initial state.

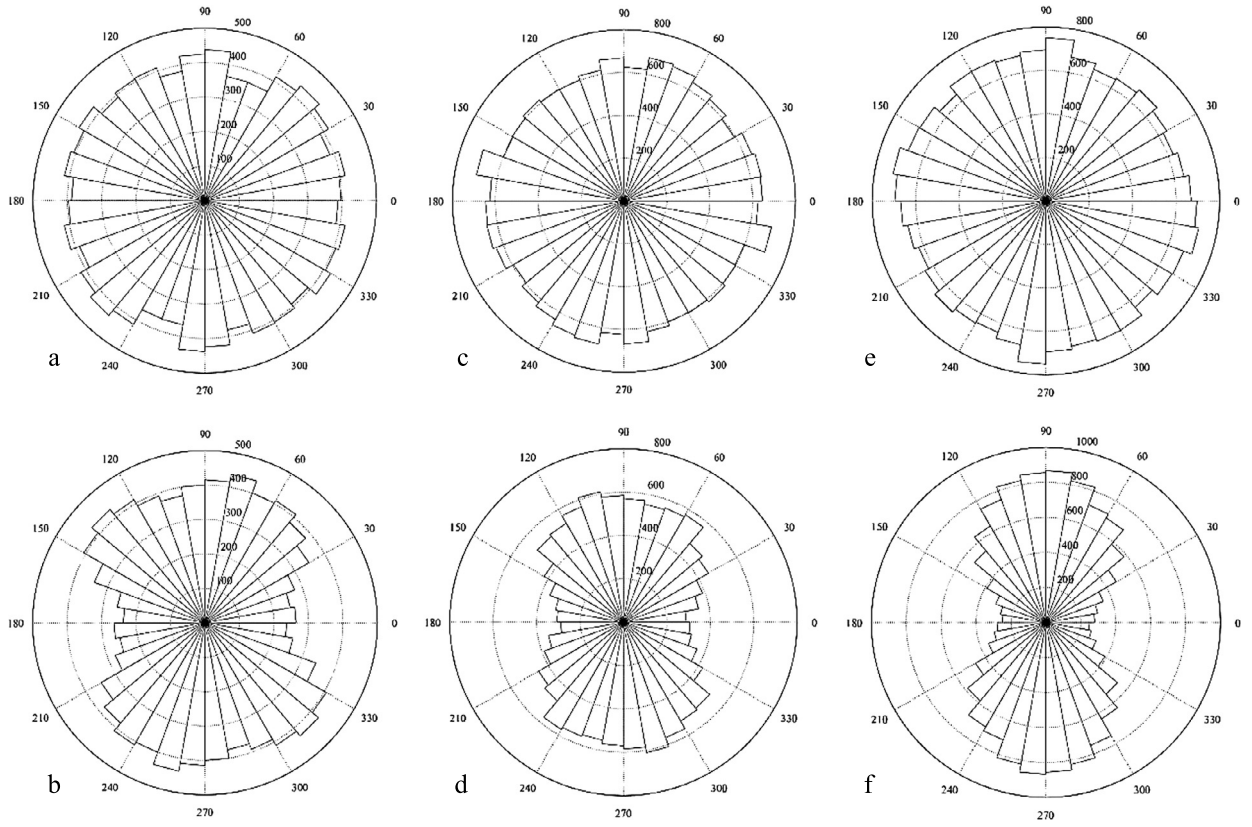

Fig. 11. Rose diagrams of contact normal with confining pressure 600 kPa: (a) circular grains at 0% of axial strain; (b) circular grains at 20% of axial strain; (c) square grains at 0% of axial strain; (d) square grains at 20% of axial strain; (e) elongated grains at 0% of axial strain; (f) elongated grains at 20% of axial strain.

However, the elongated particle has a main axis, and the square particle is isotropic. To better resist the axial loading, the elongated particles rotate to be perpendicular to the major principal stress direction (illustrated in Fig. 4c). This results in a larger number of contacts in this direction and increases the resistance to axial loading. Therefore, during deformation, the contacts of the elongated particles are larger than these of square particles, resulting in a remarkable gap between them.

Combining Figs. 14 and 18, the evolution of deviatoric stress is discussed at the microscale. Under the same confining pressure, at the initial state, there are the biggest percent of the high degree and smallest percent of the low degree for the degree distribution. And Z is near the peak point (i.e. the number of contacts is near the peak). This means that the number of contacts around the particles is the maximum among the total shearing process. To compress the sample, a big deviatoric stress is needed. So the deviatoric stress increase to the peak point rapidly. When the axial compression goes on, the percent of the high degree decreases and that of the low degree increases, and Z decreases. There is less limits on the particles. Particles can slide and roll more easily than at the initial state. Thus, the resistance gradually decreases. This resistance is steady when Z and the degree distribution are steady. On the other hand, combining Figs. 17 and 18, the different particle shapes can be analyzed. The Z of circular particles is lower than that of irregular particles, and the degree distribution of circular particles is located on the left side of irregular particles. Thus, the circular particles are more easily sliding than the irregular particles are. And it is an isotropic particle, which can roll easily. Therefore, the sample with circular particles has the smallest peak and residual deviatoric stresses. When the irregular particles are researched, the curves of the degree distribution are similar at the initial state. But the degree distribution of the elongated particles is located on the right side of that of the square particles at the critical state. The Z value of the elongated particles is bigger than that of the square particles all the time. The elongated particle has a main axis, and the square one is the isotropic particle. Thus, the elongated particles have more limits to slide and roll than square particles, and thus the specimen of elongated particles has biggest peak and residual deviatoric stresses.

4. Mesostructure evolution

4.1. Loop evolution

The example of granular assemblies, illustrated in Fig. 13b, can be treated as networks, whose nodes and edges represent particles and contact relations, respectively. The topologic structure in networks called loops is made up of edges and nodes.

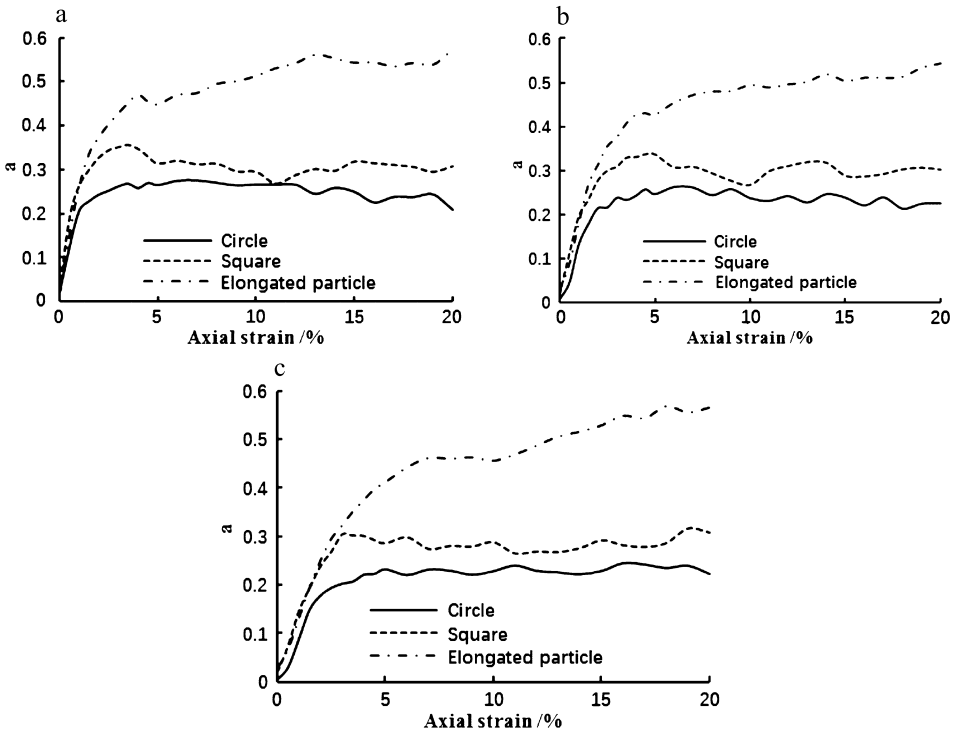

Fig. 12. Anisotropy evolution of particle assemblies: (a) confining pressure, 200 kPa; (b) confining pressure, 400 kPa; (c) confining pressure, 600 kPa.

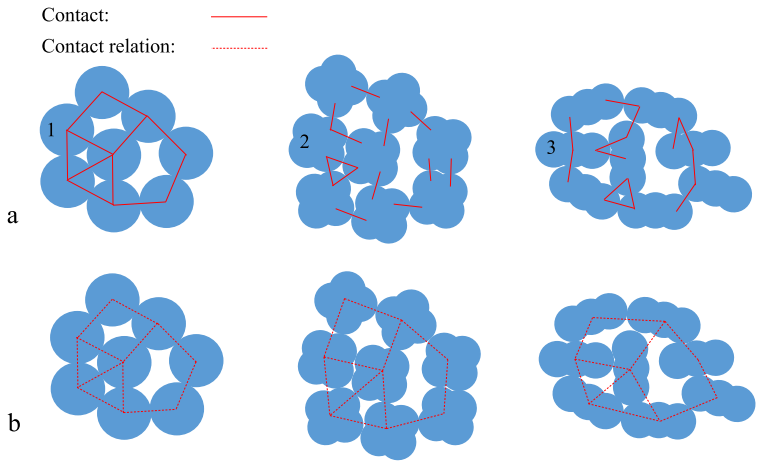

Fig. 13. (a) Degree of particles; (b) granular assemblies treated as the network.

When the loop has N edges, it is called "N loops". This definition is easy to use in samples with circular particles [24,25]. When the irregular particles are considered, the contact points between two irregular particles may be two or more than two (see Fig. 13a). In order to calculate the loop of irregular particles, the contacts between two particles should be treated as one contact relation. Thus, in Fig. 13b, these networks all have two three loops, one four loop, and one five loop. On the other hand, the property of the loop is dependent upon its side number. When the side number increases, with larger void space and more degree of freedom, the loops tend to be looser and more deformable. On the contrary, with the side number decreasing, the loops have smaller void space and there are few degrees to move. In a word, when the loop is forced to move, its nodes with different displacements, the loop transfers to other categories when the degree of freedom cannot be satisfied with the deformation.

Under a confining pressure of 200 kPa, the different loops in samples are computed, and their evolution with axial strain are illustrated in Fig. 19. There are few 11 or higher-order loops in samples, thus only 10 or lower-order loops are investigated. Here, as illustrated in Fig. 19a, 3 and 4 loops, about percent 50% in samples, dominate the topologic structure for the circular particles. And the number of 4 loops is more than one of 3 loops. When the side number of loops increases,

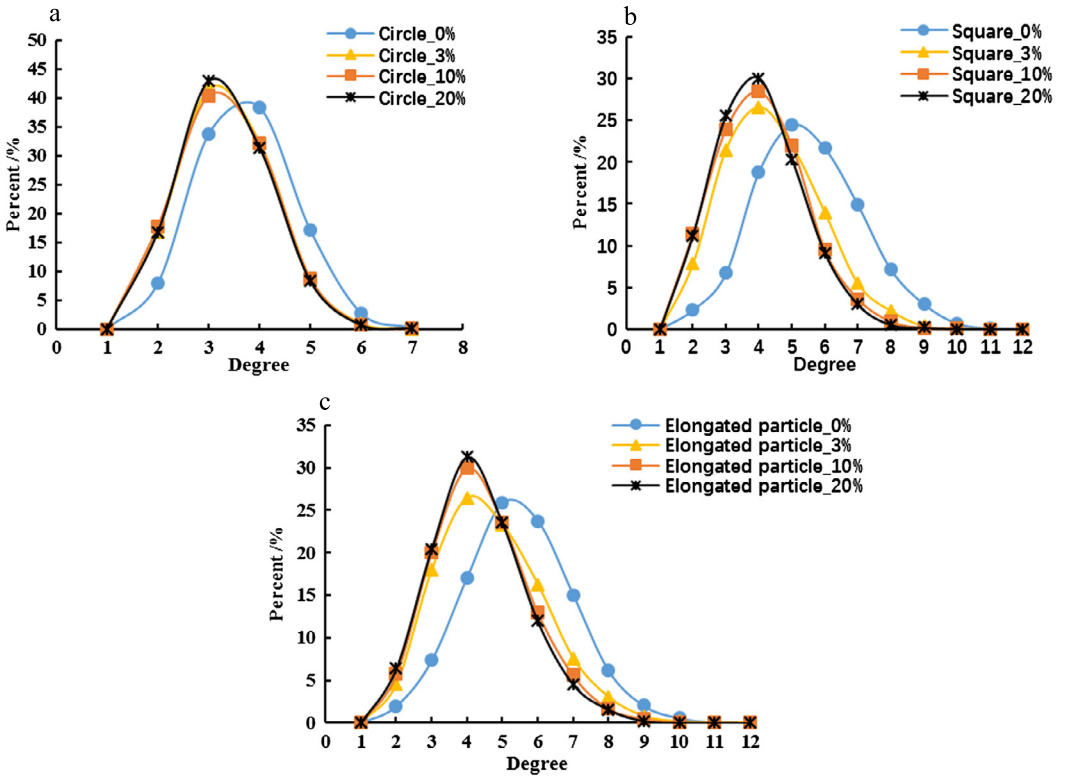

Fig. 14. Distribution of degrees under a confining pressure of 200 kPa: (a) sample with circular particles; (b) sample with square particles; (c) sample with elongated particles.

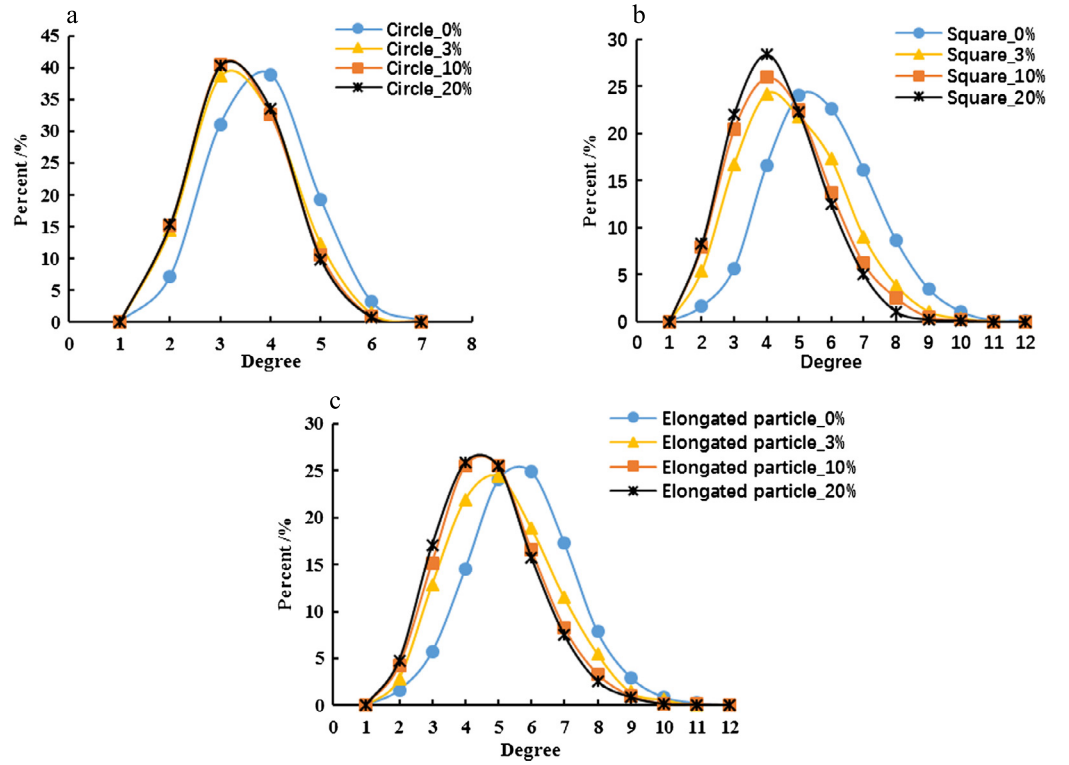

Fig. 15. Distribution of degrees under a confining pressure of 400 kPa: (a) sample with circular particles; (b) sample with square particles; (c) sample with elongated particles.

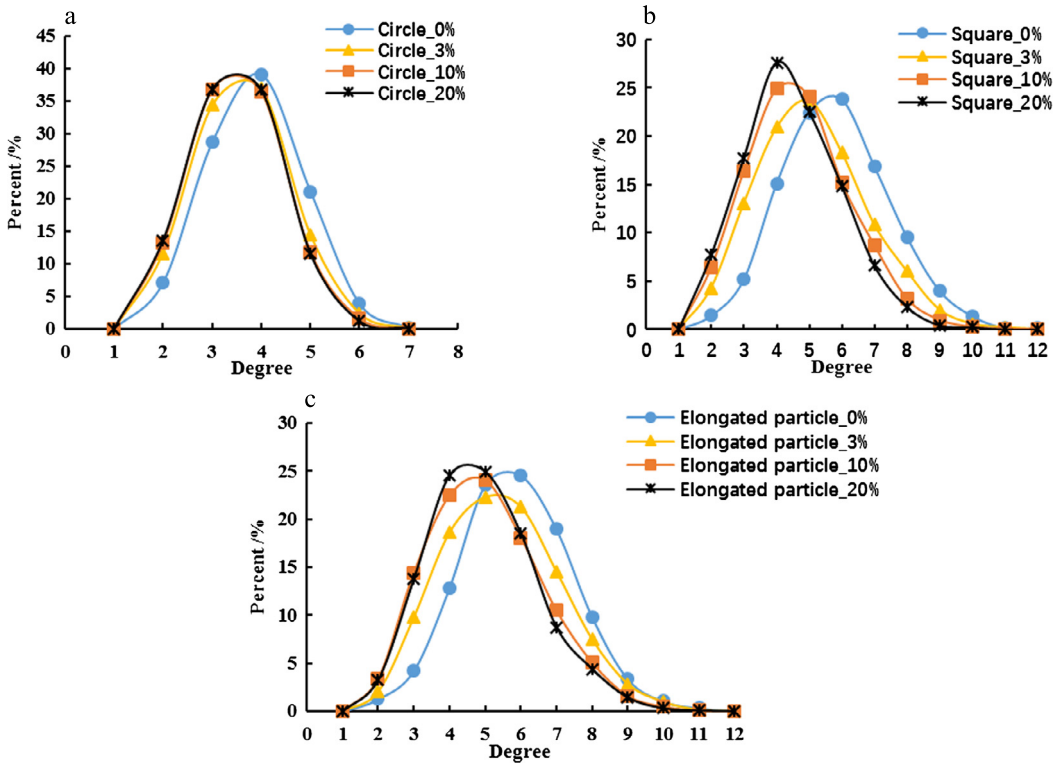

Fig. 16. Distribution of degrees under a confining pressure of 600 kPa: (a) sample with circular particles; (b) sample with square particles; (c) sample with elongated particles.

among 5 or higher-order loops, the curves of loops gradually move down. The numbers of 3, 4, and 5 loops all decrease pronouncedly at first, and with evolution of the axial strain, they oscillate around different levels. The number of 6 or higher-order loops increases pronouncedly firstly, and when the axial strain increases, they are nearly steady. These features are the same as in previous studies [24,25], which lack the loop features about irregular particles. Then, the loop features of square and elongated particles are discussed here. The loops evolution of sample with square particles is shown in Fig. 19b. These trends for loops evolution with axial strain are the same as those for the sample with circular particles, whereas the loops evolution of the sample with elongated particles shown in Fig. 19c is different from that of circular or square particles. Here, the number of 3 loops is pronouncedly larger than that of 4 loops. And the evolution of 5 loops is different from that of isotropic particles. For the one evolving with axial strain, it has a pronounced increase and then oscillates around a level. This trend is the same as that of the higher-order loops.

The amplifying diagrams taken from the samples are displayed in Fig. 20. As we can see, 3, 4 and 5 loops evolve from lower-order to higher-order with dilatancy going on. When the sample is sheared with dilatancy, the contact relations between particles disappear more than those generated. The loop with less degree of freedom (i.e. 3, 4, and 5 loops for the isotropic particles, and 3 and 4 loops for the elongated particles) which cannot be satisfied with the deformation, gradually switches to higher-order loops (i.e. 6 and higher-order loops for the isotropic particles, and 5 and higher-order loops for the elongated particles), which have more space to deform. Then the numbers that loops with lesser degree of freedom transfer to higher-order loops are equal to the ones that higher-order loops transfer to loops with lesser degree of freedom. The higher-order loops deform to have more space to satisfy the dilatancy.

When we are talking about of different particle shapes, the isotropic particles display a similar trend for the evolution of loops, whereas the elongated particles have 3 loops, which is pronouncedly more than 4 loops. And 5 loops increase at first. These are dramatically different from those of isotropic particles. 5 loops made up of elongated particles have higher degree of freedom than those for isotropic particles. When the 3 and 4 loops are considered, 3 loops can afford more forces than 4 loops. The topologic structure of the elongated particles can resist larger forces than that of the isotropic particles. At the degree discussed, we know that the microstructure of irregular particles can afford more forces than that of circular particles. Thus, once again, the peak and residual deviatoric stress of elongated particles are the largest, and those of circular particles are the smallest. Combining the degree and the loops, on the one hand, the microstructures of irregular particles are similar, whereas the one of circular particles is different from that of irregular particles. On the other hand, the mesostructures of isotropic particles are similar, but the one of elongated particles is different from that of isotropic particles.

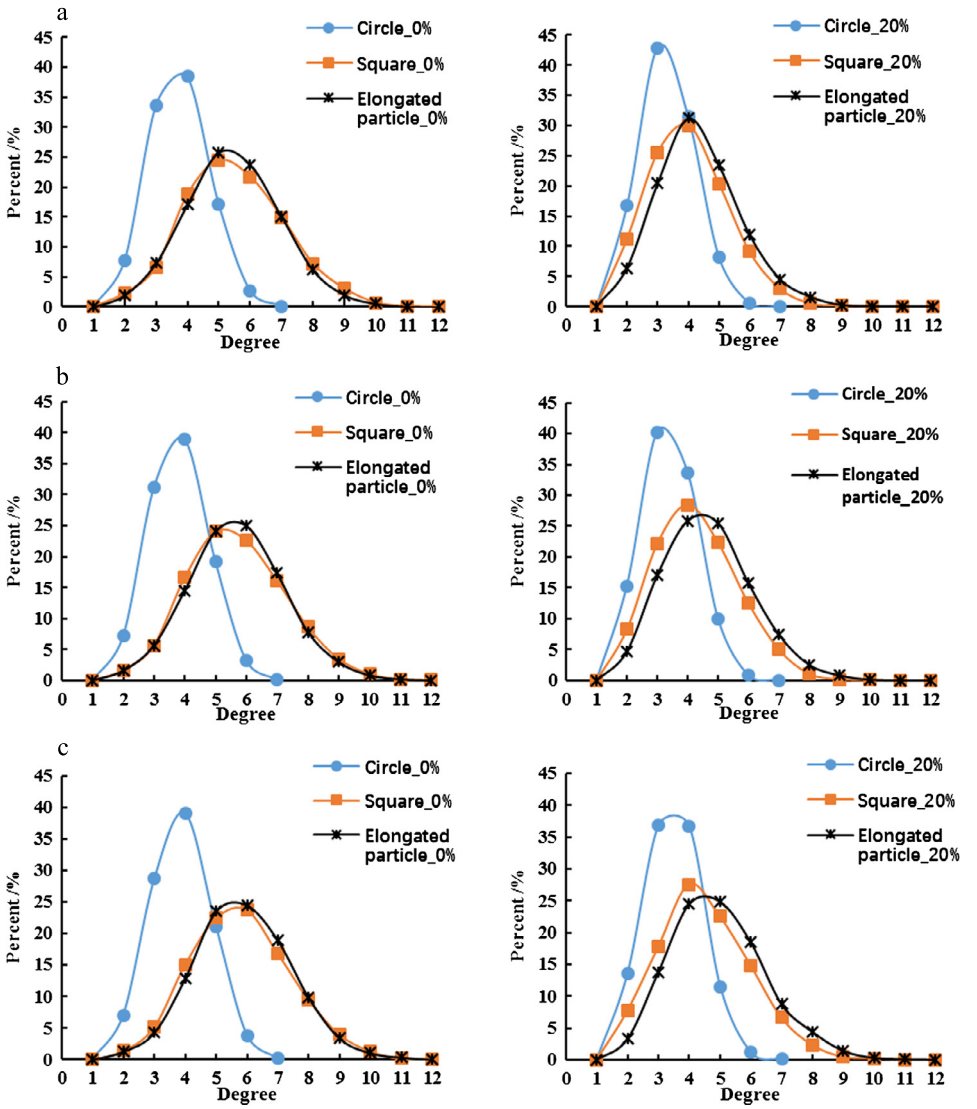

Fig. 17. The degree distribution of circular and irregular particles: (a) confining pressure, 200 kPa; (b) confining pressure, 400 kPa; (c) confining pressure, 600 kPa.

4.2. Modified clustering coefficient

The properties of the network can be researched through the complex network method. And many of the recent developments of this method have taken place in sociology, biology, and in the field of granular materials [28,43–46]. Studies have found that the 3 loops dominate the topologic structure at the mesoscale and 3 loops in a network is associated with frustrated rotations of particles and as such to stability [47,48]. In order to characterize the presence of loops of order three, the clustering coefficient in complex networks is used. Now, the definition of the clustering coefficient is introduced. The clustering coefficient of vertex i (C_i) is proposed as [49,50]:

$$C_i = \frac{2\,l_i}{k_i(k_i-1)} \tag{5}$$

Refer to Fig. 21 to understand the definition of C_i, where k_i is the number of neighbors for i, l_i represents the number of contact relations between the neighbors of i, and $k_i(k_i-1)/2$ stands for any neighbor of i connected with any other neighbor of i. Note that when the clustering coefficient of irregular particles is calculated, the contacts between two particles should be treated as one contact relation. Averaging all the C_i, the network clustering (C) is defined as [50]:

$$C = \frac{1}{N}\sum_{i=1}^{N} C_i \tag{6}$$

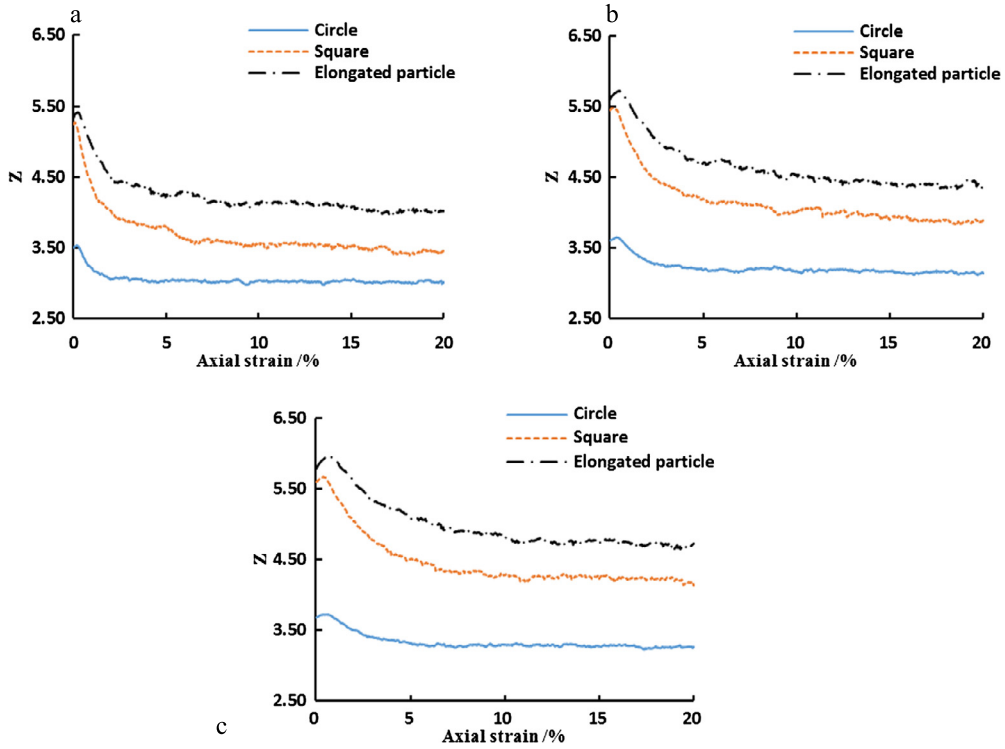

Fig. 18. Evolution of the coordination numbers for circular and irregular particles: (a) confining pressure, 200 kPa; (b) confining pressure, 400 kPa; (c) confining pressure, 600 kPa.

where N is the number of nodes in the sample. The values of C_i and C both range from 0 to 1. A high value of the clustering coefficient means a closely packed structure, whereas a low value corresponds to fewer 3 loops, loose structure, and less contacts.

For granular materials, particles too far from each other have no chance to be in contact directly, which may not be the case for other types of networks. As a result, the clustering coefficient of the vertex is strictly smaller than 1, which is not necessarily the case for other network types in which any node can be linked to any other one. Clusters for granular materials are shown in Fig. 21, and there are few vertexes totally compassed by its neighbors, so this condition is neglected in later discussions. The clustering coefficient of vertex i ranges from 0 to $2/k_i$. Then, using these C_i to calculate C through Equation (6) cannot provide the really average value, because the C_i have a weighted coefficient when the number of neighbors for i is different. Hence, combining the structure of granular materials, the modified clustering coefficient of vertex i (C_i') is proposed. By eliminating the weighted coefficient, we can make the clustering coefficient of vertex i range from 0 to 1. This modified one is proposed as:

$$C_i' = C_i \frac{k_i}{2} = \frac{l_i}{k_i - 1} \tag{7}$$

$$C' = \frac{1}{N} \sum_{i=1}^{N} C_i' \tag{8}$$

The C_i and C_i' for granular materials are contrasted in Fig. 21. C_i' and C' are more reasonable for granular materials, so they are used in later discussion.

The 2, 3, 4, 5, or 6 neighbors of the vertex are calculated using the modified clustering coefficient, respectively. Such values are illustrated in Fig. 22. Note here that the neighbor means the particle number around the center particles, which is different from the contact. On the one hand, the same particle shape is discussed at first. As we can see that the curves of C' move upward when the number of neighbors increases. All the curves decrease at first, and then fluctuate around a steady state, whereas the magnitude of the decrease increases when the number of neighbors increases. This means that the particles are denser with higher number of neighbors, and 3 loops of high number of neighbors also are pronouncedly broken. On the other hand, the effect of particle shape on the mesostructure is discussed. Each curve of C' of elongated particles is larger than that corresponding to isotropic particles, and each curve of circular particles is similar to that corresponding to square particles. Thus, the isotropic particles have similar mesostructures, and there is a difference between the elongated and isotropic particles when mesostructure is discussed. The evolution of C' for the network is

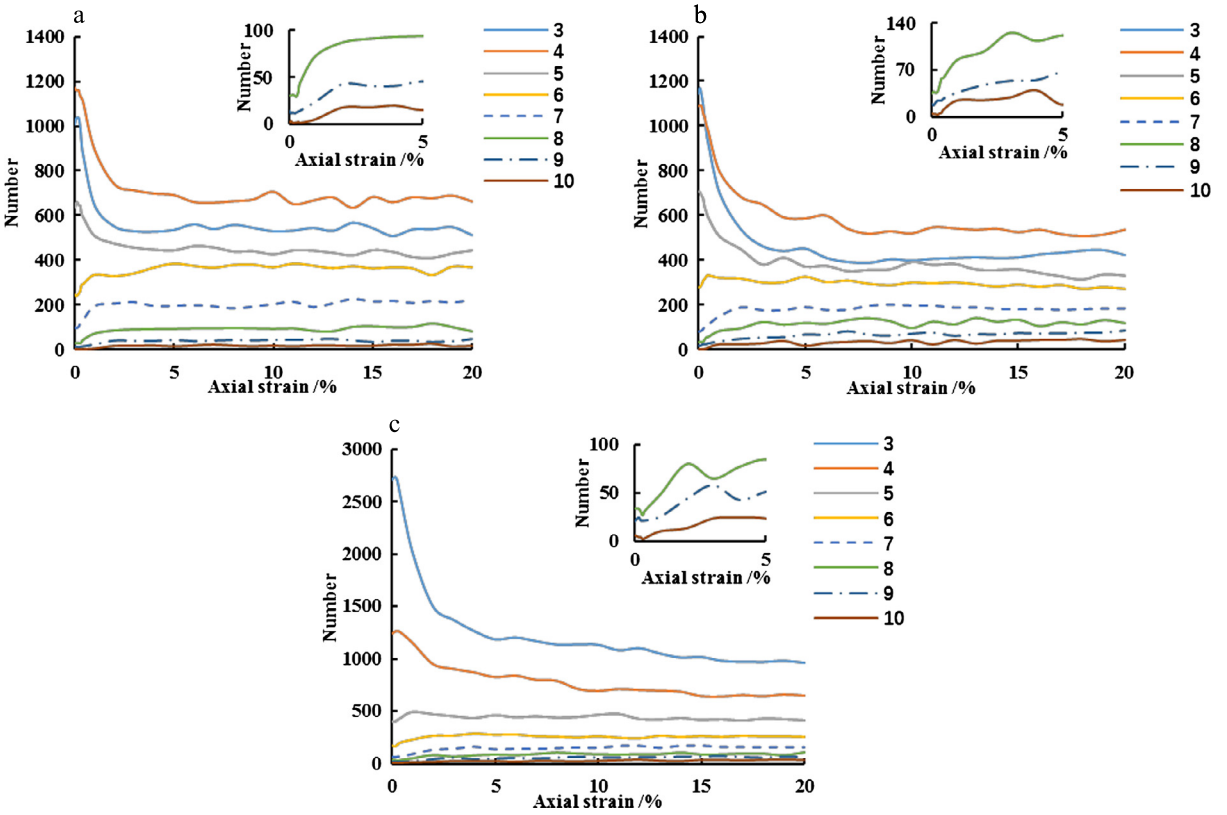

Fig. 19. Loops evolving with axial strain under a confining pressure of 200 kPa: (a) sample with circular particles; (b) sample with square particles; (c) sample with elongated particles.

shown in Fig. 23. The curves of isotropic particles are close to each other, but that of elongated particles is larger than that of isotropic particles. This demonstrates once more that 3 loops have larger ratio in elongated particles than in isotropic particles.

5. Conclusion

In this paper, with the help of DEM, the biaxial tests are used to explore the effect of particle shape, including circular, square, and elongated particles, on the macro-properties of granular materials, with attention focused on micro-scale evolving with particle shape. Hence, particle rotation, anisotropy of normal contacts and degree are discussed. Furthermore, the loops and a modified clustering coefficient are proposed to study the influence of particle shape on the mesostructure evolution of granular materials. From these analyses, the conclusions are summarized as follows.

(1) The particle shape has a pronounced influence on the macro-properties of the granular assemblies. When the value of the aspect ratio (AR) decreases, i.e. particle shape becomes more irregular, both the peak and the residual deviatoric stress increase. On the other hand, the value of dilatancy at the critical state increases when particle shape becomes irregular.

(2) The magnitude and pattern of particle rotation in samples are also influenced by particle shape. With AR decreasing, the absolute value of both the mean clockwise and counterclockwise particle rotation decrease, and the particles with rotation exceeding the mean rotation values are also discussed. Clockwise rotation is dominant in the direction that dips to the left side, and counterclockwise rotation is dominant in the direction that dips to the right side. This pattern and shear bands become obvious when particle shape becomes irregular.

(3) The characteristics of fabric evolution are remarkably different when particle shape varies. When AR decreases, the magnitude of anisotropy gradually increases. On the other hand, the average degree (Z) also increases when particle shape becomes irregular. The Z values of irregular particles, i.e. square and elongated particles, are close to each other at the initial state. The degree distributions for the irregular particles are almost the same at the initial state, but the circular particles have lower-order degree than irregular particles. At steady state, the degree distribution curves move toward higher-order degree when AR decreases, and the curves of irregular particles are very close to each other. Therefore, irregular particles have similar microstructure, and such microstructure is different from that of circular particles.

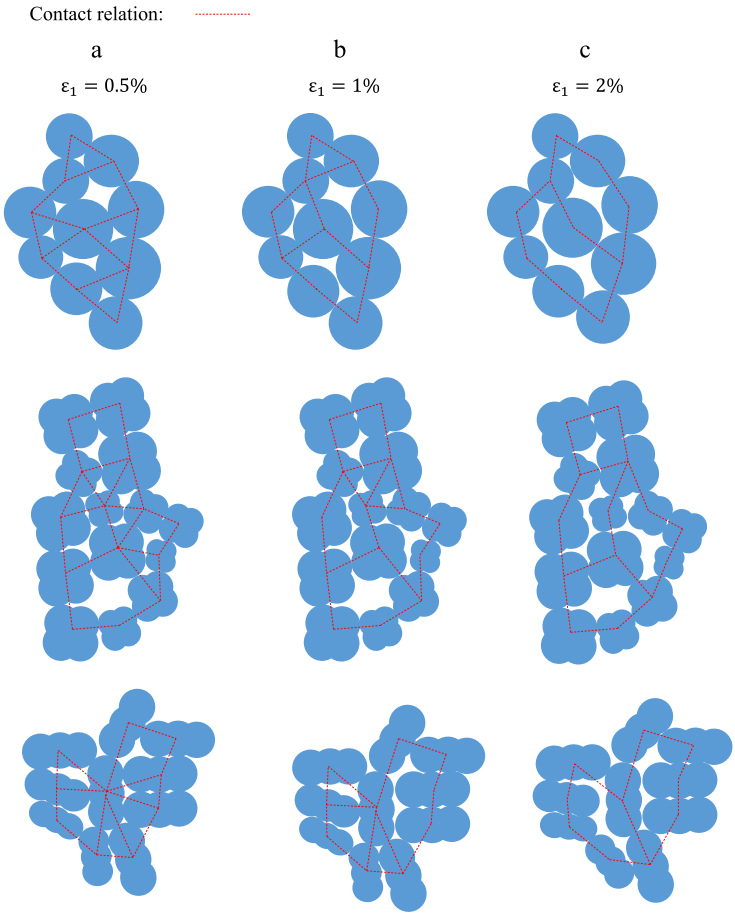

Fig. 20. Local amplifying diagram taken from samples: (a) 3 and 4 loops dominating in the sample; (b) many contact relations disappearing on horizontal direction; (c) higher-order loops generated.

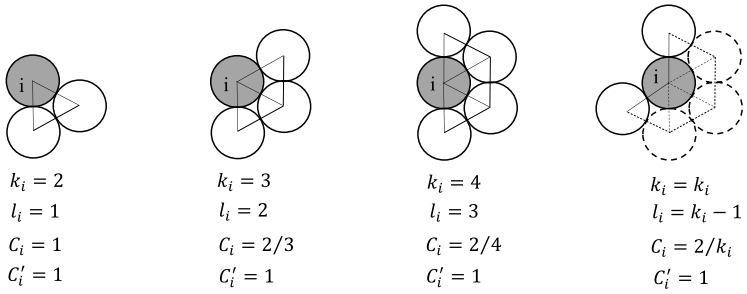

Fig. 21. Illustration of clustering coefficients and their modified version.

(4) Particle shape has also an influence on the topologic structure at mesoscale of granular materials. At the mesoscale, the isotropic particles (i.e. circular and square particles) have similar trends of loop evolution. They both have more 4 loops than 3 loops, and with axial strain evolving, 5 loops have a decrease at first and then a leveling-off, whereas the elongated particles have obviously different trends compared with the isotropic particles. The elongated particles have more 3 loops than 4 loops. And Its 5 loops have an increase at first and then a leveling-off. Hence, the isotropic particles have similar mesostructure, and such mesostructure is dramatically different from that of elongated particles.

(5) The clustering coefficient in complex networks is used to define the evolution of 3 loops in granular materials. But the original clustering coefficient is not suitable for granular materials. Thus a modified method to calculate the clustering coefficient is proposed. The results of modified clustering coefficient are also influenced by particle shape. The elongated particles have a larger value of the modified clustering coefficient than that of isotropic particles. Such values of isotropic particles are similar. These pronounced mesostructures in isotropic particles are similar, and such mesostructure is different from that of elongated particles.

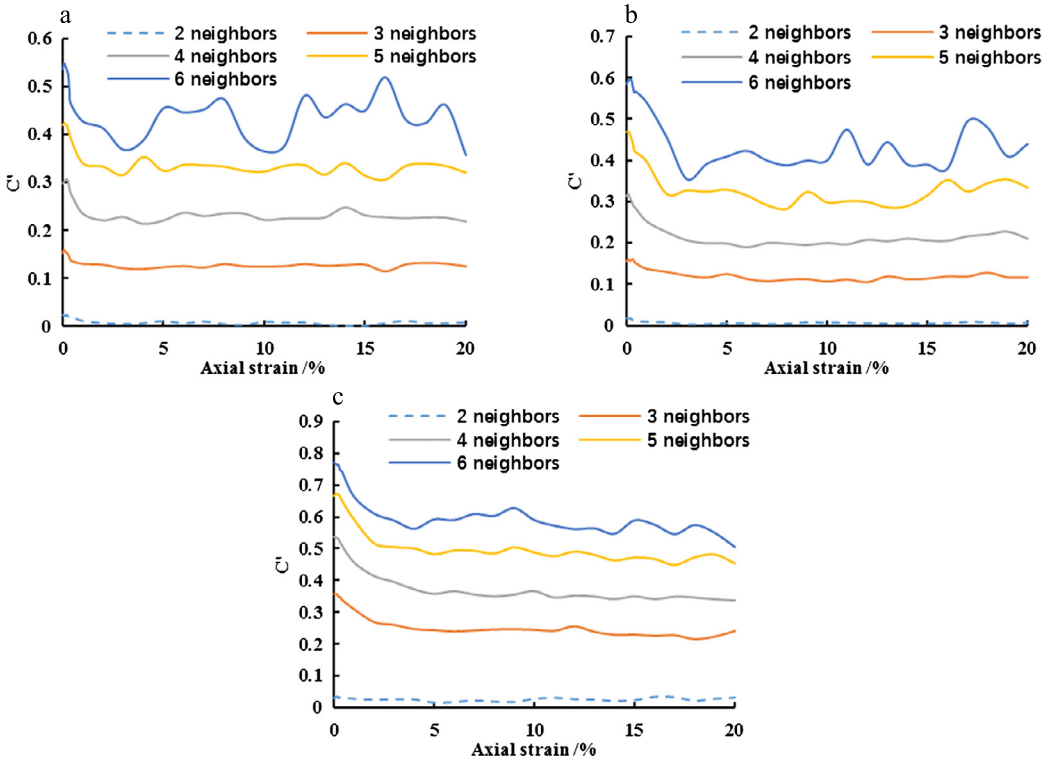

Fig. 22. Modified clustering coefficient for different neighbors around a vertex under a confining pressure of 200 kPa: (a) sample with circular particles; (b) sample with square particles; (c) sample with elongated particles.

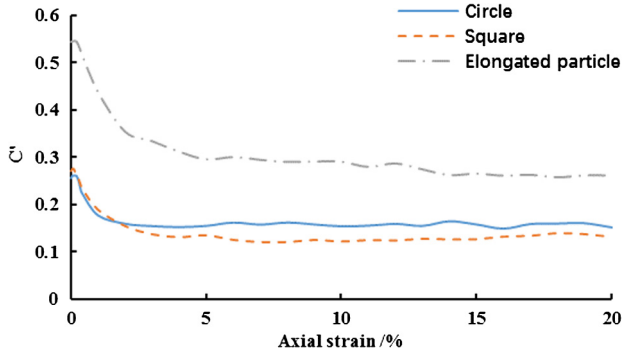

Fig. 23. Network clustering coefficients of different particle shapes under a confining pressure of 200 kPa.

It has been found that the samples composed of circular, square, and elongated particles have different properties for particle rotation, fabric evolution, and topologic structure. These results can give clues to quantify the mechanical relation between circular particles and irregular particles in further researches.

Acknowledgements

The authors appreciate the funding provided by the National Key Research and Development Program of China (Project No. 2017YFC1501003) and the CAS Pioneer Hundred Talents Program (Dr. Liu Enlong). Thanks are extended to Lian Jiang for useful discussion.

References

[1] R.C. Hidalgo, I. Zuriguel, D. Maza, I. Pagonabarraga, Role of particle shape on the stress propagation in granular packings, Phys. Rev. Lett. 103 (2009) 118001.
[2] C. Nouguier-Lehon, Effect of the grain elongation on the behaviour of granular materials in biaxial compression, C. R. Mecanique 338 (2010) 587–595.
[3] D.-H. Nguyen, E. Azéma, F. Radjai, P. Sornay, Effect of size polydispersity versus particle shape in dense granular media, Phys. Rev. E 90 (2014) 012202.

[4] Y. Yang, J.F. Wang, Y.M. Cheng, Quantified evaluation of particle shape effects from micro-to-macro scales for non-convex grains, Particuology 25 (2016) 23–35.
[5] S. Zhao, N. Zhang, X. Zhou, L. Zhang, Particle shape effects on fabric of granular random packing, Powder Technol. 320 (2017) 175–186.
[6] K. Shinohara, M. Oida, B. Golman, Effect of particle shape on angle of internal friction by triaxial compression test, Powder Technol. 107 (2000) 131–136.
[7] B. Sukumaran, A.K. Ashmawy, Quantitative characterisation of the geometry of discrete particles, Géotechnique 51 (2001) 619–627.
[8] G.C. Cho, J. Dodds, J.C. Santamarina, Particle shape effects on packing density, stiffness, and strength: natural and crushed sands, J. Geotech. Geoenviron. 132 (2006) 591–602.
[9] J. Yang, L.M. Wei, Collapse of loose sand with the addition of fines: the role of particle shape, Géotechnique 62 (2012) 1111–1125.
[10] J. Yang, X.D. Luo, Exploring the relationship between critical state and particle shape for granular materials, J. Mech. Phys. Solids 84 (2015) 196–213.
[11] P.A. Cundall, O.D.L. Strack, A discrete numerical model for granular assemblies, Géotechnique 29 (1979) 47–65.
[12] D.-H. Nguyen, E. Azéma, P. Sornay, F. Radjai, Effects of shape and size polydispersity on strength properties of granular materials, Phys. Rev. E 91 (2015) 032203.
[13] J.P. de Bono, G.R. McDowell, Investigating the effects of particle shape on normal compression and overconsolidation using DEM, Granul. Matter 18 (2016) 55.
[14] D. Höhner, S. Wirtz, V. Scherer, A study on the influence of particle shape and shape approximation on particle mechanics in a rotating drum using the discrete element method, Powder Technol. 253 (2014) 256–265.
[15] R. Maione, S.K.D. Richter, G. Mauviel, G. Wild, DEM investigation of granular flow and binary mixture segregation in a rotating tumbler: influence of particle shape and internal baffles, Powder Technol. 286 (2015) 732–739.
[16] L. Tong, Y.H. Wang, DEM simulations of shear modulus and damping ratio of sand with emphasis on the effects of particle number, particle shape, and aging, Acta Geotech. 10 (2015) 117–130.
[17] J. Tian, E. Liu, L. Jiang, X. Jiang, Y. Sun, R. Xu, Influence of particle shape on the microstructure evolution and the mechanical properties of granular materials, C. R. Mecanique 346 (2018) 460–476.
[18] W.M. Yan, Fabric evolution in a numerical direct shear test, Comput. Geotech. 36 (2009) 597–603.
[19] R. Wang, P. Fu, J.M. Zhang, Y.F. Dafalias, Evolution of various fabric tensors for granular media toward the critical state, J. Eng. Mech. 143 (2017) 04017117.
[20] M.J. Jiang, H.B. Yan, H.H. Zhu, S. Utili, Modeling shear behavior and strain localization in cemented sands by two-dimensional distinct element method analyses, Comput. Geotech. 38 (2011) 14–29.
[21] N. Estrada, E. Azéma, F. Radjai, A. Taboada, Identification of rolling resistance as a shape parameter in sheared granular media, Phys. Rev. E 84 (2011) 011306.
[22] W. Zhou, J. Liu, G. Ma, W. Yuan, X. Chang, Macroscopic and microscopic behaviors of granular materials under proportional strain path: a DEM study, Int. J. Numer. Anal. Methods Geomech. 40 (2016) 2450–2467.
[23] R.A. Hosn, L. Sibille, N. Benahmed, B. Chareyre, Discrete numerical modeling of loose soil with spherical particles and interparticle rolling friction, Granul. Matter 19 (2017) 4, https://doi.org/10.1007/s10035-016-0687-0.
[24] A. Tordesillas, D.M. Walker, Q. Lin, Force cycles and force chains, Phys. Rev. E 81 (2010) 011302.
[25] H. Zhu, F. Nicot, F. Darve, Meso-structure evolution in a 2D granular materials during biaxial loading, Granul. Matter 18 (2016) 3.
[26] H. Zhu, F. Nicot, F. Darve, Meso-structure organization in two-dimensional granular materials along biaxial loading path, Int. J. Solids Struct. 96 (2016) 25–37.
[27] L. Papadopoulos, M.A. Porter, K.E. Daniels, D.S. Bassett, Network analysis of particles and grains, J. Complex Networks 6 (4) (2018) 485–565, https://doi.org/10.1093/comnet/cny005.
[28] D.M. Walker, A. Tordesillas, Topological evolution in dense granular materials: a complex networks perspective, Int. J. Solids Struct. 47 (2010) 624–639.
[29] A. Tordesillas, P. O'Sullivan, D.M. Walker Paramitha, Evolution of functional connectivity in contact and force chain networks: feature vectors, k-cores and minimal cycles, C. R. Mecanique 338 (2010) 556–569.
[30] F. Altuhafi, C. O'Sullivan, I. Cavarretta, Analysis of an image-based method to quantify the size and shape of sand particles, J. Geotech. Geoenviron. Eng. 139 (2013) 1290–1307.
[31] S. Sheng, Y. Dou, X. Tao, S. Zhu, B. Xu, Q. Li, X. Guo, X. He, Specification of Soil Test, SL237–1999 ed., China Water and Power Press, Beijing, 1999.
[32] GDR-MiDi, On dense granular flows, Eur. Phys. J. E 14 (2004) 341–365.
[33] F. Radjai, Force and fabric states in granular media, AIP Conf. Proc. 1145 (2009) 35–42.
[34] F. Alonso-Marroquin, H.B. Muhlhaus, H.J. Herrmann, Micromechanical investigation of soil plasticity using a discrete model of polygonal particles, Theor. Appl. Mech. 35 (2008) 11–28.
[35] Z. Bi, Q. Sun, F. Jin, M. Zhang, Numerical study on energy transformation in granular matter under biaxial compression, Granul. Matter 13 (2011) 503–510.
[36] N.A. Hama, T. Ouahbi, S. Taibi, H. Souli, J.-M. Fleureau, A. Pantet, Analysis of mechanical behaviour and internal stability of granular materials using discrete element method, Int. J. Numer. Anal. Methods Geomech. 40 (2016) 1712–1729.
[37] K. Iwashita, M. Oda, Micro-deformation mechanism of shear banding process based on modified distinct element method, Powder Technol. 109 (2000) 192–205.
[38] C. O'Sullivan, J.D. Bray, S. Li, A new approach for calculating strain for particulate media, Int. J. Numer. Anal. Methods Geomech. 27 (2003) 859–877.
[39] D. Vågberg, P. Olsson, S. Teitel, Shear banding, discontinuous shear thickening, and rheological phase transitions in athermally sheared frictionless disks, Phys. Rev. E 95 (2017) 052903.
[40] M. Oda, H. Kazama, Microstructure of shear bands and its relation to the mechanisms of dilatancy and failure of dense granular soils, Géotechnique 48 (1998) 465–481.
[41] L. Rothenburg, R.J. Bathurst, Analytical study of induced anisotropy in idealized granular materials, Géotechnique 39 (1989) 601–614.
[42] N.P. Kruyt, Micromechanical study of fabric evolution in quasi-static deformation of granular materials, Mech. Mater. 44 (2012) 120–129.
[43] R. Bond, Complex networks: network healing after loss, Nat. Hum. Behav. 1 (2017) 87.
[44] J. Gao, B. Barzel, A.L. Barabási, Universal resilience patterns in complex networks, Nature 530 (2016) 307–312.
[45] P. Cao, E. Liu, L. Jiang, Evolution of the mesoscopic parameters and mechanical properties of granular materials upon loading, Math. Probl. Eng. (2017), https://doi.org/10.1155/2017/9314689.
[46] L. Jiang, E. Liu, J. Tian, X. Jiang, Effects of Inter-particle frictional coefficients on evolution of contact networks in landslide process, Engineering 9 (2017) 917–936.
[47] A. Smart, J.M. Ottino, Granular matter and networks: three related examples, Soft Matter 4 (2008) 2125–2131.
[48] A.G. Smart, J.M. Ottino, Evolving loop structure in gradually tilted two-dimensional granular packings, Phys. Rev. E 77 (2008) 041307.
[49] D.J. Watts, S.H. Strogatz, Collective dynamics of 'small-world' networks, Nature 393 (1998) 440–442.
[50] L. da, F. Costa, F.A. Rodrigues, G. Travieso, P.R. Villas Boas, Characterization of complex networks: a survey of measurements, Adv. Phys. 56 (2007) 167–242.